Slightly Depleted Lubricant-infused Surfaces Are No Longer Slippery

Christopher Vega-Sánchez[†,‡,¶] and Chiara Neto[*,†,‡]

†*School of Chemistry, The University of Sydney, NSW 2006 Australia*

‡*University of Sydney Nano Institute, The University of Sydney, NSW 2006 Australia*

¶*School of Electromechanical Engineering, Costa Rica Institute of Technology, Campus Cartago, 159-7050 Costa Rica*

E-mail: chiara.neto@sydney.edu.au

Phone: +61 2 9351 2752 . Fax: +61 2 9351 3329

Abstract

Textured surfaces infused with a lubricating fluid effectively reduce fouling and drag. These functions critically depend on the presence and distribution of the lubricant, which can be depleted by many mechanisms, including shear flow. We present a two-phase Couette flow computational dynamic simulation over lubricant-infused surfaces containing grooves oriented perpendicular to the flow direction, with the aim of revealing how interfacial slip, and therefore drag reduction, is impacted by lubricant depletion. We show that even a slight (20%) lubricant loss decreases slip to the point of making the lubricant superfluous, even for lubricants with lower viscosity than the flowing liquid and irrespective of how well the lubricant wets the grooves. We explain that the drastic slip reduction is linked to a significant increase in the total viscous dissipation and, to zero dissipation in the lubricant (similar to the one given by a no slip boundary).

Introduction

Interfacial slip at solid boundaries has attracted extensive research attention over the past two decades, as slip allows fluids to flow faster at the solid boundary and, therefore, reduces the large frictional drag that opposes flow on the nano- and microscale.[1,2] Interfacial slip is quantified with the slip length b, which is the imaginary distance beyond the solid wall at which the linear extrapolation of the fluid velocity vanishes to zero. A way to increase slip is to replace the fluid-solid contact with a fluid-fluid contact, which has been achieved with lubricant-infused surfaces (LIS): superhydrophobic surfaces (hydrophobic structured surfaces in which the cavities in the topography are infused with gas) or liquid-infused surfaces (infused with a liquid lubricant).[3–10] The measured slip length values on LIS are sufficiently large to have a significant effect on microfluidic flows.[1–3,11–14]

On LIS, regions of small intrinsic slip (originating from low molecular interactions between the solid wall and the working fluid) are interspersed with regions of large slip (in which the working fluid is in contact with the lubricant, gas or liquid). The latter scenario is called apparent slip, because it is a consequence of the lubricating effect of the (low-viscosity) infused gas/liquid.[15] Large local slip, however, does not translate always into an overall slip effect. Gas pockets, or even shear-free interfaces, could produce a no-slip condition if rough enough[16–19] or if contaminated with impurities.[20] Consequently, LIS are usually characterized by an effective slip length, which is the equivalent slip required on a smooth surface that would produce the same flow conditions far away from the composite surface.

Previous models[16–18,21–31] have shown that the effective slip in LIS depends on lubricant area fraction, cavity aspect ratio (to a certain extent), fluid-lubricant viscosity ratio μ_r, and lubricant contact angle θ (see Fig. 1(a)). These models assume that the fluid-fluid interface is pinned at the top of the surface topography, is flat and/or non-deformable. However, under realistic conditions, the interface is not pinned at the top of the surface topography[20,32] and lubricant depletion occurs due to the shear stress or static pressure imposed by the external fluid.[7,32–39] The impact of a partially filled cavity on slip has not been fully investigated,

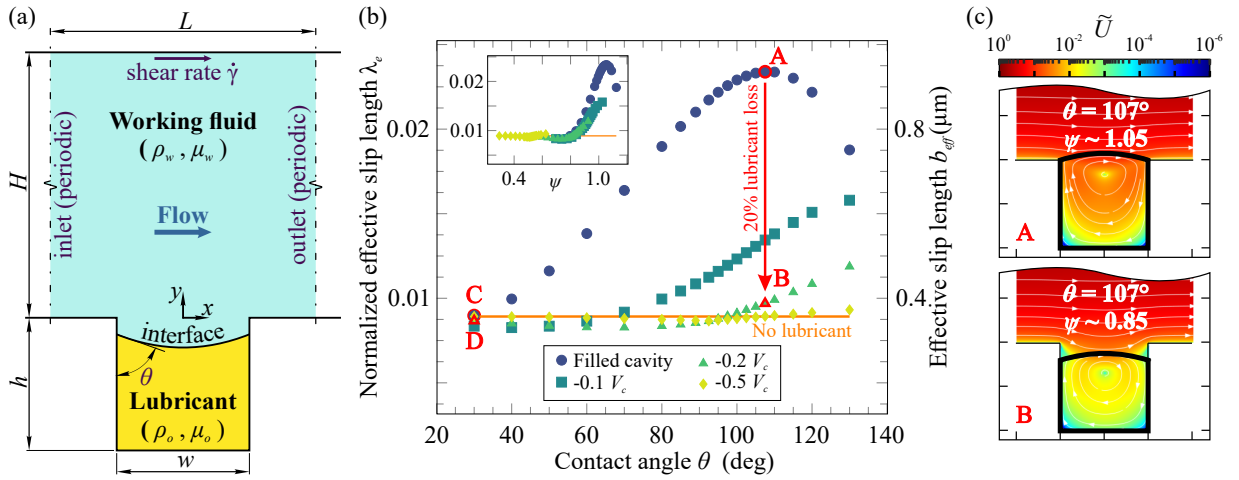

Figure 1: (a) Definition of parameters used to model Couette flow over transverse grooves. The flow is driven by a shear rate applied at the upper wall ($y = H$) in the x-direction only. The grooves extend infinitely out of the plane. This schematic shows a case in which the groove is partially filled with lubricant. (b) Normalized effective slip length λ_e (left y-axis) and dimensional effective slip length b_{eff} for $H = 40$ μm (right y-axis) versus contact angle θ for different cavity filling and $\mu_r = 10$. From top to bottom, the symbols represent a fully filled cavity and partially filled cavities with lubricant loss of 10, 20 and 50% of the cavity volume V_c. The horizontal solid orange line is the case with no lubricant in the groove (i.e. single phase flow) and the working fluid fully wetting the cavity. The inset shows λ_e as a function of the lubricant filling ratio ψ and the symbols and colors correspond to the legend showed in the main panel. (c) Normalized velocity magnitude $\tilde{U} = U/u_{in}$ for the cases labeled A and B in (b), with streamlines shown in white. The lubricant volume is highlighted with a thick black line. Cases C and D are shown in Fig. S2.

despite this scenario being highly relevant to physical experiments and important for the design of LIS.

In this study, we found that the effective slip on LIS containing grooves oriented perpendicular to the flow direction is severely affected by lubricant depletion. A 20% lubricant loss reduces the effective slip to the point where the remaining 80% of the lubricant becomes superfluous. Given that in experiments a certain degree of lubricant depletion is observed to occur, the large slip reported previously in LIS[6,7,40,41] is difficult to explain with the presence of the lubricant alone. We recently showed that spontaneous nucleation of nanobubbles on LIS enhances slip and explains the large slip observed.[10]

Here we further corroborate this recent result, showing that, in realistic scenarios, the

presence of the (depleted) lubricant alone is unlikely to explain the large slip observed in LIS. We report numerical simulations to quantify the effective fluid slip over a LIS in which grooves perpendicular to the flow direction are filled (or partially filled) with a lubricant, as shown in Fig. 1(a). The effect of lubricant filling ratio ψ and lubricant contact angle θ on the effective slip is explored by modeling an interface that is not pinned at the top of the groove. The filling ratio is defined as $\psi = V_o/V_c$, where V_o and $V_c = wh$ (see Fig. 1(a)) correspond to the lubricant and cavity volume, respectively. The numerical model by Ge et al.[42] considered the effect of a cavity partially filled with lubricant, but only for two lubricant contact angle values, corresponding to slightly concave or convex interfaces. Ageev et al.[43,44] studied the effect of gas depletion in superhydrophobic surfaces on effective slip, but only considered the limit case in which the shear stress on the curved bubble surface vanishes. Here we consider the effect of the viscous dissipation in the lubricant and demonstrate that a high interface curvature only reduces slip when the cavity is fully filled with lubricant.

The model

In the simulation domain (Fig. 1(a)) the working fluid (viscosity μ_w and density ρ_w) flows over a groove infused with a lubricant (viscosity μ_o and density ρ_o). The flow is driven by a shear stress in the x-direction $\tau = \mu_w \dot{\gamma}$ imposed on the upper wall, where $\dot{\gamma}$ is the shear rate. All the solid walls are assumed to hold a no-slip condition. The deformation of the fluid-lubricant interface was calculated numerically so as to satisfy the prescribed static contact angle of the lubricant with the wall θ, the working fluid-lubricant interfacial tension σ and the shear rate $\dot{\gamma}$. Unless specified, parameters common in microfluidic experiments on LIS were used:[4] $L = 20\,\mu\text{m}$, $H = 2L$, $h = w = L/2$, $\rho_r = \rho_w/\rho_o = 1.07$ (see Supporting Information, SI, for explanation), $\sigma = 40\ \text{mN}\,\text{m}^{-1}$ (interfacial tension of silicone oil-water), and $\mu_o = 7.6$ mPa s; the shear rate was adjusted to achieve a volumetric flow rate of $100\,\mu\text{L}\,\text{min}^{-1}\,\text{m}^{-1}$ across all the simulations. The phase-field method[45] was used for tracking the working

fluid-lubricant interface, and the continuity and momentum equations of an incompressible Newtonian fluid flow were solved:

$$\nabla \cdot \mathbf{u} = 0, \tag{1}$$

$$\rho \frac{\partial \mathbf{u}}{\partial t} + \rho(\mathbf{u} \cdot \nabla)\mathbf{u} = \nabla \cdot [-p\mathbf{I} + \mu(\nabla \mathbf{u} + \nabla \mathbf{u}^T)] + \mathbf{F_{st}}, \tag{2}$$

where $\mathbf{u} = (u(x, y), v(x, y))$ is the velocity, t is time, $\mathbf{F_{st}}$ is the imposed external force derived from the phase-field method for representing the interfacial tension σ; ρ and μ are the density and viscosity, respectively, and are defined as $\rho = \rho_w + (\rho_o - \rho_w)V_f$ and $\mu = \mu_w + (\mu_o - \mu_w)V_f$. V_f the volume fraction of the lubricant ($V_f = 0$ represents the working fluid, while $V_f = 1$ the lubricant). Given that the phase-field method is employed, the interface has a finite thickness (see[45] and SI), which is defined to be thin in comparison with the overall size of the domain (around few nanometers), to guarantee that the interface is sharp enough to simulate an interface between two immiscible fluids. The lubricant mass was monitored over time to guarantee the mass conservation of both fluids throughout the simulation, which in turn validates the correctness of the model.

At each coordinate (x, y) the fluid velocity magnitude is computed as $U(x, y) = \sqrt{u^2 + v^2}$. Additionally, the height-average velocity at the inlet u_{in} is computed as $u_{in} = \frac{1}{H}\int_0^H u(-L/2, y)\, dy$. The discretization of the domain was refined to the point where the results became mesh-independent.

A fully filled cavity, in which the contact points of the interface with the wall are located at the corners of the groove, and a partially filled cavity, in which the interface is free to move at $y < 0$ before finding the steady-state position (see reference system in Fig. 1(a)), were simulated. For a given contact angle θ, the filled cavity case contains the maximum lubricant volume allowed in the cavity without overflow. In the partially filled cavity case, lubricant depletion was simulated by reducing the lubricant volume by 10, 20 and 50% of the cavity volume V_c, irrespective of θ (ψ instead varies with θ). The normalized effective slip

length λ_e was quantified as $\lambda_e = \frac{\overline{u}(H)}{\dot{\gamma}H} - 1$, where $\overline{u}(y) = \dot{\gamma}(y + \lambda_e H)$ is the average velocity as a function of y (i.e. $\overline{u}(y) = \frac{1}{L}\int_{-L/2}^{+L/2} u(x,y)\,dx$), assuming a linear velocity profile with a slip length $b_{eff} = \lambda_e H$. The reference slip plane was defined to be at $y = 0$. All the results presented here correspond to the case in which the system has reached the steady-state condition.

Results and discussion

For the fully filled case, our model reproduces accurately the results obtained with previous analytical and numerical models for different viscosity ratios (see Fig. S1),[16,18,21,25,26] which demonstrates the validity of the method. Briefly, our results show that the effective slip length depends on the lubricant contact angle and reaches a maximum value for a slightly protruding interface, at lubricant contact angle around $\theta = 107°$, and increases with increasing viscosity ratio. Also, for $\mu_r < 1$ the presence of the lubricant reduces the effective slip compared to the case with no lubricant (i.e. single phase flow). Most importantly, these results show that for a wetting lubricant ($\theta \sim 30°$) which produces a highly concave interface, the slip length is no larger than in the case with no lubricant at all, irrespective of the viscosity of the lubricant (i.e. μ_r). This finding highlights a direct conflict with the common practice of selecting lubricants which fully wet the solid substrate (with low contact angle) to increase lubricant retention in LIS.[38]

Fig. 1(b) presents the effect of lubricant loss on effective slip length λ_e as a function of the contact angle θ. Here, $\mu_r = 10$ was chosen as it represents a realistic scenario in which the lubricant is a liquid. However, these results can be extrapolated for $\mu_r > 1$, including superhydrophobic surfaces, for which $\mu_r \sim 50$ when the working fluid is water (however, it must be considered that Eq. 1 clearly applies only for incompressible lubricants). As shown in Fig. 1(b), lubricant loss of just 10% of the cavity volume V_c induces a drastic decrease of the slip length. In the worst case ($\theta = 107°$), a lubricant reduction of only $10\%V_c$ decreases

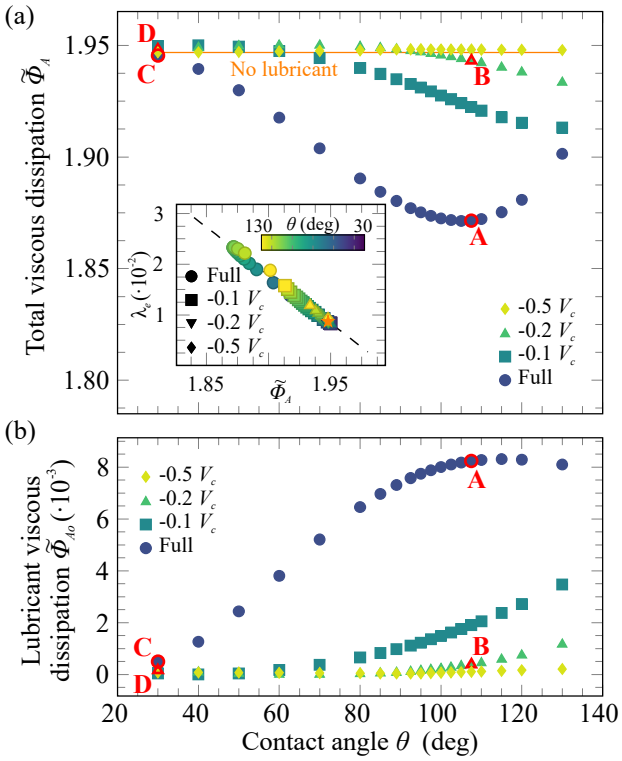

Figure 2: (a) Normalized total viscous dissipation $\tilde{\Phi}_A$, summing over both the working fluid and lubricant, as a function of lubricant contact angle θ. The horizontal solid orange line corresponds to the case with no lubricant in the groove (i.e. single phase flow). The inset shows the slip length λ_e versus the viscous dissipation $\tilde{\Phi}_A$ (orange star represents the case of no lubricant in the cavity). (b) Normalized viscous dissipation in the lubricant $\tilde{\Phi}_{Ao}$ as a function of lubricant contact angle θ. Both panels are for viscosity ratio $\mu_r = 10$. The viscous dissipation for the fully filled case for different μ_r is shown in Fig. S3.

λ_e by $\sim 50\%$. When the lubricant loss is 20% and 50% of V_c, the values of λ_e are equal to those obtained when there is no lubricant in the cavity ((i.e. single phase flow, orange line in Fig. 1(b)). In these cases, the maximum reduction of λ_e reaches $\sim 60\%$, and on average is 50%. This is an unexpected result given that the remaining large portion of the lubricant in the cavity is 10 times less viscous than the working fluid, so, based on viscosity alone, it would be expected to provide higher apparent slip. Once the lubricant loss is larger than 20% of V_c, the decrease in λ_e is the same irrespective of the contact angle θ and therefore the shape of the interface. Indeed, the inset in Fig. 1(b) shows that λ_e is much more sensitive to changes in the filling ratio ψ than of θ, meaning that lubricant depletion affects the slip length more than the shape of the interface itself. Despite these results being for a case in

which $\mu_r = 10$, they are also in agreement with the ones presented by[43] for a case in which $\mu_r \to \infty$.

Four representative points (A, B, C and D) are chosen in Fig. 1(b), and the velocity profile for A and B is shown on Fig. 1(c). Point A at $\theta = 107°$, which is around the maximum λ_e, has a highly mobile lubricant, denoted by the orange and red colors ($\tilde{U} = 1 - 10^{-1}$). By comparison, point B (with 20% less lubricant) shows a decrease of one order of magnitude in the lubricant velocity, denoted by the more yellow color range ($\tilde{U} = 10^{-2}$). Surprisingly, λ_e is the same for points C and D, despite D having 20% less lubricant than C. For $\theta = 30°$ (points C and D), the velocity magnitude is around one to two orders of magnitude smaller in comparison with A (Fig. S2).

For a fully filled cavity, a slightly concave or convex interface offers a ball bearing effect to the working fluid and, therefore, enhances the overall slip in the system. However, strongly concave interfaces ($\theta \sim 30°$) lose this effect as the working fluid is forced to enter into the cavity, as shown by the strongly bent streamlines in C in Fig. S2. On the other hand, although highly convex interfaces ($\theta > 120°$) provide a good ball bearing effect, they are also an obstacle for the flow, which negatively impacts λ_e.[16,46] For the partially filled case, the ball bearing effect is decreased by the fact that the interface is below the corners of the cavity, causing the working fluid to enter into the cavity, similar to the case of a concave interface. Fig. 1(b) highlights the overwhelming effect of filling ratio on slip, which needs to be explained with a physical mechanism.

We were able to explain this effect by calculating the viscous dissipation rate Φ in the lubricant and the working fluid separately. For incompressible Newtonian fluid flows, the viscous dissipation rate per unit volume can be estimated as:[47]

$$\Phi = 2\mu_i \left[\left(\frac{\partial u_x}{\partial x} \right)^2 + \left(\frac{\partial u_y}{\partial y} \right)^2 \right] + \mu_i \left[\frac{\partial u_y}{\partial x} + \frac{\partial u_x}{\partial y} \right]^2, \tag{3}$$

where μ_i is the viscosity of the $i-$fluid (working fluid or lubricant). The total dissipation in the domain of area A (including the area occupied by both, the working fluid and the

lubricant) is calculated as follows:

$$\Phi_A = \iint_A \Phi \, dA. \tag{4}$$

The dissipation is normalized as $\tilde{\Phi} = \Phi H^2/u_{in}^2\mu_w$ and $\tilde{\Phi}_A = \Phi_A/u_{in}^2\mu_w$, where u_{in} is the height-average velocity at the inlet.

Fig. 2(a) shows the total viscous dissipation $\tilde{\Phi}_A$ as a function of the contact angle θ, and explains the mechanism underpinning slip for both fully filled and partially filled cavities. The total viscous dissipation is a minimum for a fully filled cavity and for $\theta \approx 107°$. This is why a slightly protruding interface, and not a flat one with $\theta = 90°$, provides the maximum slip length, as shown by.[46] However, as the amount of lubricant decreases in the cavity from full to 50% less lubricant volume, the total viscous dissipation approaches the case of no lubricant in the system (i.e. single phase flow). Again, this occurs irrespective of lubricant contact angle, as observed in Fig. 2(a).

Given that the viscous dissipation is a measure of the irreversible conversion from kinetic to internal energy in the system, the configurations with lower total viscous dissipation are expected to transport the fluid more efficiently. The key result is that the total viscous dissipation $\tilde{\Phi}_A$ and the effective slip length λ_e are inversely related for all the lubricant volumes tested, as shown the inset in Fig. 2(a).

For a better understanding, the viscous dissipation distribution for a fully filled case (i.e. interface located at the top of the cavity) is plotted for three representatives cases in Fig. 3. First, both concave and convex interfaces cause the fluid flow to deviate from the straight path as observed by the bending of the streamlines (black lines in the Fig. 3). However, the concave interface ($\theta = 80°$) produces a downward displacement of the streamlines which results in a large oval region of moderate dissipation ($\tilde{\Phi} \sim 4 - 5$) directly on top of the interface. This is highlighted by the white dashed lines in Fig. 3. Interestingly, this oval region of moderate dissipation decreases in size as the interface becomes more convex. Indeed, in the highly convex interface ($\theta = 130°$) the oval completely disappears, indicating lower

viscous dissipation in the bulk fluid.

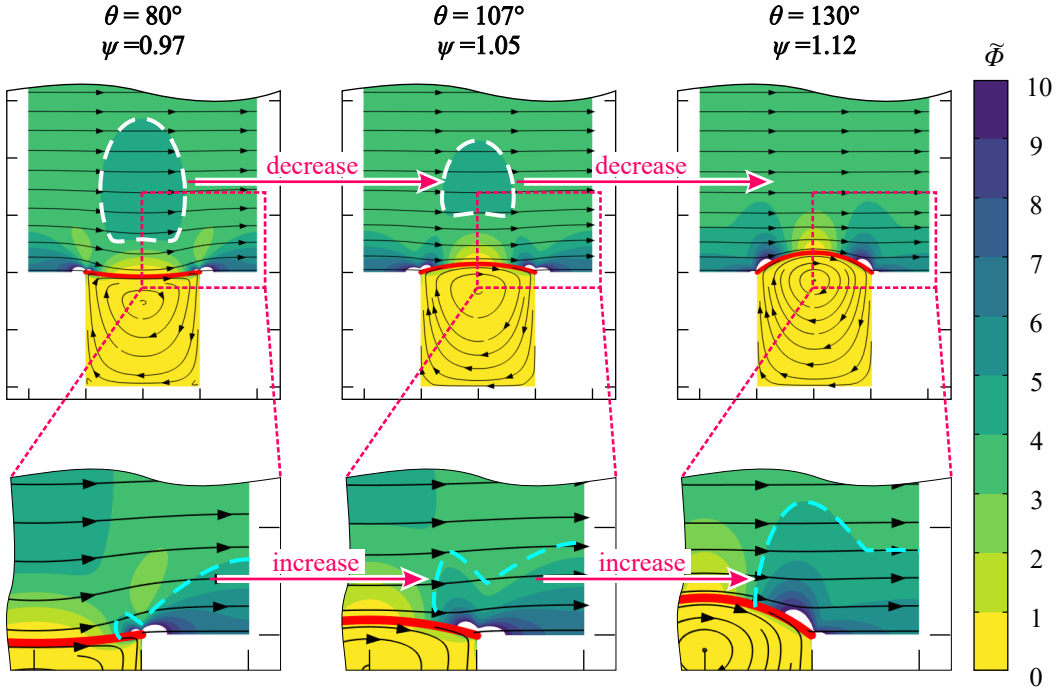

Figure 3: Distribution of the normalized viscous dissipation rate $\tilde{\Phi}$ for a fully filled case for $\mu_r = 10$ and three representative cases: a concave interface ($\theta = 80°$), a slightly convex interface ($\theta = 107°$) and a highly convex interface ($\theta = 130°$). Streamlines are represented by black lines. The fluid-lubricant interface is showed as a red thick line. The dashed lines are a guide to the eye for the comparison between cases. All panels share the same scale bar. White regions correspond to values of $\tilde{\Phi} > 10$.

More intriguing still is the fact that at $\theta = 80°$ and $\theta = 130°$ the slip length is the same, as shown in Fig. 1(b). In these two cases the total viscous dissipation is the same, as shown in Fig. 2(a). Although the viscous dissipation in the bulk fluid is low for $\theta = 130°$, near the wall the dissipation is high, as shown in the close-up images in Fig. 3 and highlighted by the cyan dashed lines. This is an indication of the lubricant-fluid interface increasing the local velocity of the fluid near the wall but at the same time acting as an obstacle for the fluid flow. Indeed, for $\theta = 130°$ the viscous dissipation near the wall is the highest of the three cases analyzed here. More protruding interfaces (e.g., $\theta > 130°$) are expected to worsen the situation, as they display even smaller slip length values as predicted by the model of Davis and Lauga.[18] Finally, the slightly convex interface ($\theta = 107°$) is a balance between these two

extreme conditions. It permits the flow to accelerate near the wall, increasing the interfacial velocity and increasing the viscous dissipation only locally, and does not act as an obstacle, resulting in a small oval region of viscous dissipation within the bulk. As a result, a slightly convex interface produces the largest slip length possible. This result also shows that that for the cavity aspect ratio studied here (i.e. $w = h$), the slip length is mainly controlled by the viscous dissipation occurring at the edge of the groove, as explained in[46] and.[48]

For a fully filled cavity, one can suggest that slightly concave or convex interfaces offer a ball bearing effect to the working fluid and, therefore, enhance the overall slip in the system. However, strongly concave interfaces ($\theta < 80°$) lose this effect as the working fluid is forced to enter into the cavity, as discussed later. On the other hand, although highly convex interfaces ($\theta > 115°$) provide a good ball bearing effect, they also represent an obstacle for the flow, which negatively impacts slip.[16,46]

In Fig. 2(b) the viscous dissipation occurring only in the lubricant $\tilde{\Phi}_{Ao}$ is plotted against the contact angle θ. Counter intuitively, $\tilde{\Phi}_{Ao}$ is higher for the fully filled case, in which the total viscous dissipation $\tilde{\Phi}_A$ in the system is the lowest, and the effective slip length λ_e is maximum. Similarly, $\tilde{\Phi}_{Ao}$ is virtually zero when the lubricant loss is 50% of V_c, which surprisingly correspond to the highest $\tilde{\Phi}_A$, as shown in Fig. 2(a). Also, $\tilde{\Phi}_{Ao}$ tends to zero as θ approaches 30°, irrespective of the volume of lubricant in the cavity. Consistently with these results for a partially filled cavity, the slip length for a fully filled cavity is inversely proportional to the total viscous dissipation, irrespective of the viscosity ratio (Fig. S3).

For highly concave interfaces ($\theta \sim 30°$), the low lubricant viscous dissipation occurring in the lubricant is mainly due to the low velocity magnitude of the lubricant, as shown in Fig. S2. As the interface becomes more concave, the lubricant becomes less mobile and loses its ability to facilitate the flow of the external fluid. This behaviour justifies why the effective slip in cases with highly concave interfaces approaches the case with no lubricant in the cavity (i.e. single phase flow, see Fig. 1(b)), as it is the external fluid entering the cavity which produces the apparent slip. The latter scenario was experimentally demonstrated by.[20] This

effect is further detailed in Fig. 4(c-d) showing the distribution of viscous dissipation rate $\tilde{\Phi}$ for points C and D.

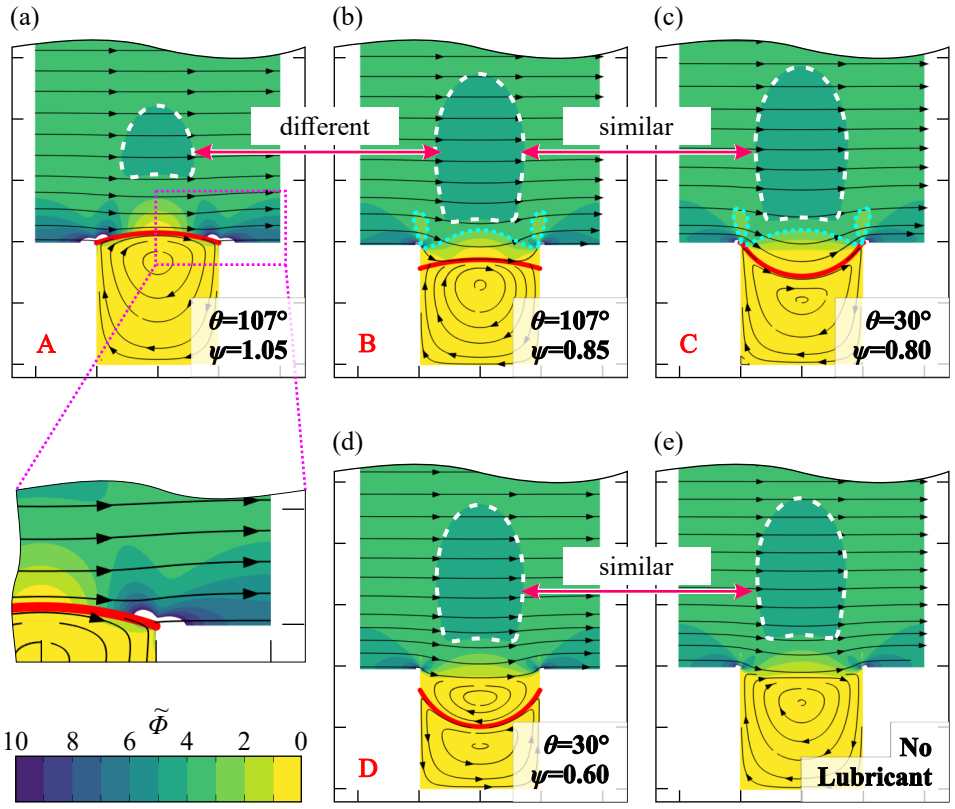

Figure 4: Distribution of the normalized viscous dissipation rate $\tilde{\Phi}$ for partially filled cases for (a)-(d) points A, B, C and D in Fig. 1, and (e) the case with no lubricant in the groove (i.e. single phase flow). The fluid-lubricant interface is showed as a red thick line. The dashed lines are a guide to the eye for the comparison between cases. All panels share the same scale bar. White regions correspond to values of $\tilde{\Phi} > 10$.

The viscous dissipation distribution for case A, the case with the maximum slip length, differs from every other case shown in Fig. 4 in that it is the only case in which the interface (or the cavity) does not represent an obstacle to the external fluid, i.e. the composite surface roughness remains low, thanks to the position and curvature of the interface. All the other cases in 4(b-e) display essentially the same effective slip length (as shown in Fig. 1(b)), despite having significantly different conditions of flow. In all cases other than A, the total viscous dissipation is higher than A because the area over which the velocity field is affected, directly above the fluid-lubricant interface, is larger than in A, as shown by the large oval

region of intermediate dissipation (dark green, $\tilde{\Phi}$ = 5-6 highlighted with a white dashed line in Fig. 4(b)-(d)).

In A there is narrow region near the cavity with high local viscous dissipation (blue and white regions, $\tilde{\Phi} > 9$, in close up in Fig. 4(a)) due to the local increase of velocity magnitude as the fluid flows from a no-slip to a partial slip condition, but overall the velocity field is not significantly perturbed by the presence of the lubricant interface and the viscous dissipation in the bulk fluid remains low. Indeed, the streamlines in the working fluid in A remain almost straight, while they are perturbed in all other cases. Even in the case of case D, where a recirculation area within the working fluid occurs inside the groove, the total viscous dissipation is similar to the other three cases. The reason is that, in depleted cases, most of the slip effect originates from the external fluid itself entering the cavity. As mentioned earlier, in these cases the velocity magnitude of the lubricant is low, and the lubricating effect can be seen as originating from a cavity of low aspect ratio (h/w) fully filled with the external fluid. This finding supports the results obtained by[26] predicting that a shallow cavity could achieve similar slip as a deep one. Indeed, the viscous distribution in the bulk fluid in cases B to D is very similar to that in the case with no lubricant in the cavity (i.e. single phase flow, see Fig. 4(e)).

Conclusions

Our results show that the lubricant contact angle and the position of the lubricant-fluid interface determine the lubricant volume in the cavity (i.e. the lubricant filling ratio), and that filling ratio dominates the effective slip on lubricant-infused surfaces containing grooves oriented perpendicular to the flow direction. The slip length reaches the maximum value when the fluid-lubricant interface is slightly protruding from the cavity ($\theta \approx 107\ ^\circ$), but only when the lubricant fully (or almost fully) fills the cavity and $\mu_r > 1$. Even a small (20% of V_c) reduction of the lubricant volume, which in a physical experiment easily occurs as a result

of depletion under flow or incomplete initial infusion of the surface, causes a drastic decrease of the effective slip and almost removes the dependence of slip on interface curvature. A $\sim 20\%$ lubricant loss produces an effective slip that is as low as when no lubricant is present (i.e. single phase flow). The total viscous dissipation rate in the system explains this result, as a slight decrease of the lubricant filling ratio significantly increases the overall energy dissipation irrespective of the interface curvature, which in turn reduces interfacial slip. The increase in viscous dissipation is qualitatively revealed by perturbations in the direction of the flow streamlines and changes in the magnitude of the velocity in the working fluid.

Given the strong sensitivity of the effective slip length to a small lubricant loss, it might be surprising that LIS have been found to be so effective at reducing drag in laminar and turbulent flow.[6,7,40,41] Our recent study on silicone oil-infused Teflon nanowrinkles revealed that drag reduction in LIS could be explained with an additional mechanism of slip, namely flow over spontaneously nucleated surface nanobubbles.[10] In situations in which the lubricant alone is expected to provide drag reduction, unless lubricant depletion can be eliminated, one must question the benefit of infusing the lubricant in LIS containing grooves oriented perpendicular to the flow direction, as the working fluid filling the cavity might be just as effective.

Acknowledgement

The authors thank the University of Sydney and the Australian Research Council Future Fellowship (FT180100214) for funding. C.V. thanks the Costa Rican Ministry of Science and Technology and Tecnologico de Costa Rica for funding.

Supporting Information Available

Validation of the numerical model, velocity profiles for highly concave interfaces and viscous dissipation for a fully impregnated surface are presented as supporting information.

References

(1) Neto, C.; Evans, D.; Bonaccurso, E.; Butt, H.-J.; Craig, V. Boundary slip in Newtonian liquids: a review of experimental studies. *Rep. Prog. Phys.* **2005**, *68*, 32859–2897.

(2) Lauga, E.; Brenner, M.; Stone, H. In *Springer Handbook of Experimental Fluid Mechanics*; Tropea, C., Yarin, A. L., Foss, J. F., Eds.; Springer Berlin Heidelberg: Berlin, Heidelberg, 2007; pp 1219–1240.

(3) Lee, C.; Choi, C.-H.; Kim, C.-J. Superhydrophobic drag reduction in laminar flows: a critical review. *Exp. Fluids* **2016**, *57*, 1–20.

(4) Vega-Sánchez, C.; Neto, C. Pressure drop measurements in microfluidic devices: a review on the accurate quantification of interfacial slip. *Adv. Mater. Interf.* **2021**, *9*, 2101641.

(5) Zhao, X.; Best, A.; Liu, W.; Koynov, K.; Butt, H.-J.; Schönecker, C. Irregular, nanostructured superhydrophobic surfaces: Local wetting and slippage monitored by fluorescence correlation spectroscopy. *Phys. Rev. Fluids* **2021**, *6*, 054004.

(6) Solomon, B. R.; Khalil, K. S.; Varanasi, K. K. Drag reduction using lubricant-impregnated surfaces in viscous laminar flow. *Langmuir* **2014**, *30*, 10970–10976.

(7) Kim, J.-H.; Rothstein, J. P. Delayed lubricant depletion on liquid-infused randomly rough surfaces. *Exp. Fluids* **2016**, *57*, 81.

(8) Scarratt, L. R.; Zhu, L.; Neto, C. How Slippery are SLIPS? Measuring Effective Slip on Lubricated Surfaces with Colloidal Probe Atomic Force Microscopy. *Langmuir* **2019**, *35*, 2976–2982.

(9) Scarratt, L. R.; Zhu, L.; Neto, C. Large Effective Slip on Lubricated Surfaces Measured with Colloidal Probe AFM. *Langmuir* **2020**, *36*, 6033–6040.

(10) Vega-Sánchez, C.; Peppou-Chapman, S.; Zhu, L.; Neto, C. Nanobubbles explain the large slip observed on lubricant-infused surfaces. *Nature Comm.* **2022**, *13*, 351.

(11) Bocquet, L.; Charlaix, E. *Chem. Soc. Rev.* **2010**, *39*, 1073–1095.

(12) Rothstein, J. P. Slip on superhydrophobic surfaces. *Annu. Rev. Fluid Mech.* **2010**, *42*, 89–109.

(13) Lee, T.; Charrault, E.; Neto, C. Interfacial slip on rough, patterned and soft surfaces: A review of experiments and simulations. *Adv. Colloid Interface Sci.* **2014**, *210*, 21–38.

(14) Hardt, S.; McHale, G. Flow and drop transport along liquid-infused surfaces. *Annual Review of Fluid Mechanics* **2022**, *54*, 83–104.

(15) Vinogradova, O. Slippage of water over hydrophobic surfaces. *Int. J. Miner. Process.* **1999**, *56*, 31–60.

(16) Steinberger, A.; Cottin-Bizonne, C.; Kleimann, P.; Charlaix, E. High friction on a bubble mattress. *Nat. Mater.* **2007**, *6*, 665–668.

(17) Hyväluoma, J.; Harting, J. Slip flow over structured surfaces with entrapped microbubbles. *Phys. Rev. Lett.* **2008**, *100*, 246001.

(18) Davis, A. M.; Lauga, E. Geometric transition in friction for flow over a bubble mattress. *Phys. Fluids* **2009**, *21*, 011701.

(19) Richardson, S. On the no-slip boundary condition. *J. Fluid Mech.* **1973**, *59*, 707–719.

(20) Bolognesi, G.; Cottin-Bizonne, C.; Pirat, C. Evidence of slippage breakdown for a superhydrophobic microchannel. *Physics of Fluids* **2014**, *26*, 082004.

(21) Philip, J. R. Flows satisfying mixed no-slip and no-shear conditions. *Z. Angew. Math. Phys.* **1972**, *23*, 353–372.

(22) Philip, J. R. Integral properties of flows satisfying mixed no-slip and no-shear conditions. *Z. Angew. Math. Phys.* **1972**, *23*, 960–968.

(23) Lauga, E.; Stone, H. A. Effective slip in pressure-driven Stokes flow. *J. Fluid Mech.* **2003**, *489*, 55–77.

(24) Ybert, C.; Barentin, C.; Cottin-Bizonne, C.; Joseph, P.; Bocquet, L. Achieving large slip with superhydrophobic surfaces: Scaling laws for generic geometries. *Phys. Fluids* **2007**, *19*, 123601.

(25) Hyväluoma, J.; Kunert, C.; Harting, J. Simulations of slip flow on nanobubble-laden surfaces. *J. Phys.: Condens. Matter* **2011**, *23*, 184106.

(26) Schönecker, C.; Baier, T.; Hardt, S. Influence of the enclosed fluid on the flow over a microstructured surface in the Cassie state. *J. Fluid Mech.* **2014**, *740*, 168–195.

(27) Sun, R.; Ng, C.-O. Effective slip for flow through a channel bounded by lubricant-impregnated grooved surfaces. *Theor. Comput. Fluid Dyn.* **2017**, *31*, 189–209.

(28) Alinovi, E.; Bottaro, A. Apparent slip and drag reduction for the flow over superhydrophobic and lubricant-impregnated surfaces. *Phys. Rev. Fluids* **2018**, *3*, 124002.

(29) Asmolov, E. S.; Nizkaya, T. V.; Vinogradova, O. I. Enhanced slip properties of lubricant-infused grooves. *Phys. Rev. E* **2018**, *98*, 033103.

(30) Asmolov, E. S.; Nizkaya, T. V.; Vinogradova, O. I. Flow-driven collapse of lubricant-infused surfaces. *Journal of Fluid Mechanics* **2020**, *901*.

(31) Zuo, H.; Javadpour, F.; Deng, S.; Li, H. Liquid slippage on rough hydrophobic surfaces with and without entrapped bubbles. *Phys. Fluids* **2020**, *32*, 082003.

(32) Kim, T. J.; Hidrovo, C. Pressure and partial wetting effects on superhydrophobic friction reduction in microchannel flow. *Phys. Fluids* **2012**, *24*, 112003.

(33) Samaha, M. A.; Vahedi Tafreshi, H.; Gad-el Hak, M. Modeling drag reduction and meniscus stability of superhydrophobic surfaces comprised of random roughness. *Phys. fluids* **2011**, *23*, 012001.

(34) Samaha, M. A.; Tafreshi, H. V.; Gad-el Hak, M. Influence of flow on longevity of superhydrophobic coatings. *Langmuir* **2012**, *28*, 9759–9766.

(35) Samaha, M. A.; Vahedi Tafreshi, H.; Gad-el Hak, M. Sustainability of superhydrophobicity under pressure. *Phys. Fluids* **2012**, *24*, 112103.

(36) Wexler, J. S.; Jacobi, I.; Stone, H. A. Shear-driven failure of liquid-infused surfaces. *Phys. Rev. Lett.* **2015**, *114*, 168301.

(37) Liu, Y.; Wexler, J. S.; Schönecker, C.; Stone, H. A. Effect of viscosity ratio on the shear-driven failure of liquid-infused surfaces. *Phys. Rev. Fluids* **2016**, *1*, 074003.

(38) Peppou-Chapman, S.; Hong, J. K.; Waterhouse, A.; Neto, C. Life and death of liquid-infused surfaces: a review on the choice, analysis and fate of the infused liquid layer. *Chem. Soc. Rev.* **2020**, *49*, 3688–3715.

(39) Peppou-Chapman, S.; Neto, C. Depletion of the Lubricant from Lubricant-Infused Surfaces due to an Air/Water Interface. *Langmuir* **2021**, *37*, 3025–3037.

(40) Lee, S. J.; Kim, H. N.; Choi, W.; Yoon, G. Y.; Seo, E. A nature-inspired lubricant-infused surface for sustainable drag reduction. *Soft Matter* **2019**, *15*, 8459–8467.

(41) Rosenberg, B. J.; Van Buren, T.; Fu, M. K.; Smits, A. J. Turbulent drag reduction over air-and liquid-impregnated surfaces. *Phys. Fluids* **2016**, *28*, 015103.

(42) Ge, Z.; Holmgren, H.; Kronbichler, M.; Brandt, L.; Kreiss, G. Effective slip over partially filled microcavities and its possible failure. *Phys. Rev. Fluids* **2018**, *3*, 1–12.

(43) Ageev, A.; Golubkina, I.; Osiptsov, A. Application of boundary element method to Stokes flows over a striped superhydrophobic surface with trapped gas bubbles. *Physics of Fluids* **2018**, *30*, 012102.

(44) Ageev, A.; Osiptsov, A. Stokes flow in a microchannel with superhydrophobic walls. *Fluid Dynamics* **2019**, *54*, 205–217.

(45) Yue, P.; Feng, J. J.; Liu, C.; Shen, J. A diffuse-interface method for simulating two-phase flows of complex fluids. *J. Fluid Mech.* **2004**, *515*, 293–317.

(46) Haase, A. S.; Wood, J. A.; Lammertink, R. G.; Snoeijer, J. H. Why bumpy is better: the role of the dissipation distribution in slip flow over a bubble mattress. *Phys. Rev. Fluids* **2016**, *1*, 054101.

(47) Bird, R. B.; Stewart, W. E.; Lightfoot, E. N. *Transport Phenomena*, second edition ed.; John-Wiley & Sons, Inc.: United States of America, 2002.

(48) Dubov, A. L.; Nizkaya, T. V.; Asmolov, E. S.; Vinogradova, O. I. Boundary conditions at the gas sectors of superhydrophobic grooves. *Physical Review Fluids* **2018**, *3*, 014002.

TOC Graphic

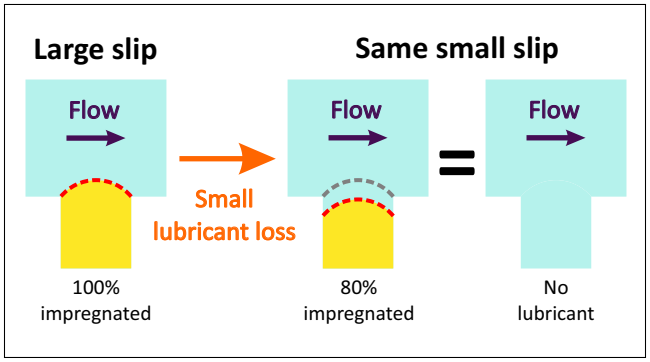
Large slip
Same small slip
Flow
Flow
Flow
Small
lubricant loss
100%
impregnated
80%
impregnated
No
lubricant